

Search for  $B^+ \rightarrow \mu^+ \nu_\mu$  and  $B^+ \rightarrow \ell^+ \nu_\ell \gamma$  decays

K. Abe,<sup>10</sup> K. Abe,<sup>47</sup> N. Abe,<sup>50</sup> I. Adachi,<sup>10</sup> H. Aihara,<sup>49</sup> M. Akatsu,<sup>24</sup> H. An,<sup>57</sup>  
 Y. Asano,<sup>54</sup> T. Aso,<sup>53</sup> V. Aulchenko,<sup>2</sup> T. Aushev,<sup>14</sup> T. Aziz,<sup>45</sup> S. Bahinipati,<sup>6</sup>  
 A. M. Bakich,<sup>44</sup> Y. Ban,<sup>36</sup> M. Barbero,<sup>9</sup> A. Bay,<sup>20</sup> I. Bedny,<sup>2</sup> U. Bitenc,<sup>15</sup> I. Bizjak,<sup>15</sup>  
 S. Blyth,<sup>29</sup> A. Bondar,<sup>2</sup> A. Bozek,<sup>30</sup> M. Bračko,<sup>22,15</sup> J. Brodzicka,<sup>30</sup> T. E. Browder,<sup>9</sup>  
 M.-C. Chang,<sup>29</sup> P. Chang,<sup>29</sup> Y. Chao,<sup>29</sup> A. Chen,<sup>26</sup> K.-F. Chen,<sup>29</sup> W. T. Chen,<sup>26</sup>  
 B. G. Cheon,<sup>4</sup> R. Chistov,<sup>14</sup> S.-K. Choi,<sup>8</sup> Y. Choi,<sup>43</sup> Y. K. Choi,<sup>43</sup> A. Chuvikov,<sup>37</sup>  
 S. Cole,<sup>44</sup> M. Danilov,<sup>14</sup> M. Dash,<sup>56</sup> L. Y. Dong,<sup>12</sup> R. Dowd,<sup>23</sup> J. Dragic,<sup>23</sup>  
 A. Drutskoy,<sup>6</sup> S. Eidelman,<sup>2</sup> Y. Enari,<sup>24</sup> D. Epifanov,<sup>2</sup> C. W. Everton,<sup>23</sup> F. Fang,<sup>9</sup>  
 S. Fratina,<sup>15</sup> H. Fujii,<sup>10</sup> N. Gabyshev,<sup>2</sup> A. Garmash,<sup>37</sup> T. Gershon,<sup>10</sup> A. Go,<sup>26</sup>  
 G. Gokhroo,<sup>45</sup> B. Golob,<sup>21,15</sup> M. Grosse Perdekamp,<sup>38</sup> H. Guler,<sup>9</sup> J. Haba,<sup>10</sup> F. Handa,<sup>48</sup>  
 K. Hara,<sup>10</sup> T. Hara,<sup>34</sup> N. C. Hastings,<sup>10</sup> K. Hasuko,<sup>38</sup> K. Hayasaka,<sup>24</sup> H. Hayashii,<sup>25</sup>  
 M. Hazumi,<sup>10</sup> E. M. Heenan,<sup>23</sup> I. Higuchi,<sup>48</sup> T. Higuchi,<sup>10</sup> L. Hinz,<sup>20</sup> T. Hojo,<sup>34</sup>  
 T. Hokuue,<sup>24</sup> Y. Hoshi,<sup>47</sup> K. Hoshina,<sup>52</sup> S. Hou,<sup>26</sup> W.-S. Hou,<sup>29</sup> Y. B. Hsiung,<sup>29,\*</sup>  
 H.-C. Huang,<sup>29</sup> T. Igaki,<sup>24</sup> Y. Igarashi,<sup>10</sup> T. Iijima,<sup>24</sup> A. Imoto,<sup>25</sup> K. Inami,<sup>24</sup> A. Ishikawa,<sup>10</sup>  
 H. Ishino,<sup>50</sup> K. Itoh,<sup>49</sup> R. Itoh,<sup>10</sup> M. Iwamoto,<sup>3</sup> M. Iwasaki,<sup>49</sup> Y. Iwasaki,<sup>10</sup> R. Kagan,<sup>14</sup>  
 H. Kakuno,<sup>49</sup> J. H. Kang,<sup>57</sup> J. S. Kang,<sup>17</sup> P. Kapusta,<sup>30</sup> S. U. Kataoka,<sup>25</sup> N. Katayama,<sup>10</sup>  
 H. Kawai,<sup>3</sup> H. Kawai,<sup>49</sup> Y. Kawakami,<sup>24</sup> N. Kawamura,<sup>1</sup> T. Kawasaki,<sup>32</sup> N. Kent,<sup>9</sup>  
 H. R. Khan,<sup>50</sup> A. Kibayashi,<sup>50</sup> H. Kichimi,<sup>10</sup> H. J. Kim,<sup>19</sup> H. O. Kim,<sup>43</sup> Hyunwoo Kim,<sup>17</sup>  
 J. H. Kim,<sup>43</sup> S. K. Kim,<sup>41</sup> T. H. Kim,<sup>57</sup> K. Kinoshita,<sup>6</sup> P. Koppenburg,<sup>10</sup> S. Korpar,<sup>22,15</sup>  
 P. Križan,<sup>21,15</sup> P. Krokovny,<sup>2</sup> R. Kulasiri,<sup>6</sup> C. C. Kuo,<sup>26</sup> H. Kurashiro,<sup>50</sup> E. Kurihara,<sup>3</sup>  
 A. Kusaka,<sup>49</sup> A. Kuzmin,<sup>2</sup> Y.-J. Kwon,<sup>57</sup> J. S. Lange,<sup>7</sup> G. Leder,<sup>13</sup> S. E. Lee,<sup>41</sup>  
 S. H. Lee,<sup>41</sup> Y.-J. Lee,<sup>29</sup> T. Lesiak,<sup>30</sup> J. Li,<sup>40</sup> A. Limosani,<sup>23</sup> S.-W. Lin,<sup>29</sup> D. Liventsev,<sup>14</sup>  
 J. MacNaughton,<sup>13</sup> G. Majumder,<sup>45</sup> F. Mandl,<sup>13</sup> D. Marlow,<sup>37</sup> T. Matsuishi,<sup>24</sup>  
 H. Matsumoto,<sup>32</sup> S. Matsumoto,<sup>5</sup> T. Matsumoto,<sup>51</sup> A. Matyja,<sup>30</sup> Y. Mikami,<sup>48</sup>  
 W. Mitaroff,<sup>13</sup> K. Miyabayashi,<sup>25</sup> Y. Miyabayashi,<sup>24</sup> H. Miyake,<sup>34</sup> H. Miyata,<sup>32</sup> R. Mizuk,<sup>14</sup>  
 D. Mohapatra,<sup>56</sup> G. R. Moloney,<sup>23</sup> G. F. Moorhead,<sup>23</sup> T. Mori,<sup>50</sup> A. Murakami,<sup>39</sup>  
 T. Nagamine,<sup>48</sup> Y. Nagasaka,<sup>11</sup> T. Nakadaira,<sup>49</sup> I. Nakamura,<sup>10</sup> E. Nakano,<sup>33</sup> M. Nakao,<sup>10</sup>  
 H. Nakazawa,<sup>10</sup> Z. Natkaniec,<sup>30</sup> K. Neichi,<sup>47</sup> S. Nishida,<sup>10</sup> O. Nitoh,<sup>52</sup> S. Noguchi,<sup>25</sup>  
 T. Nozaki,<sup>10</sup> A. Ogawa,<sup>38</sup> S. Ogawa,<sup>46</sup> T. Ohshima,<sup>24</sup> T. Okabe,<sup>24</sup> S. Okuno,<sup>16</sup> S. L. Olsen,<sup>9</sup>  
 Y. Onuki,<sup>32</sup> W. Ostrowicz,<sup>30</sup> H. Ozaki,<sup>10</sup> P. Pakhlov,<sup>14</sup> H. Palka,<sup>30</sup> C. W. Park,<sup>43</sup>  
 H. Park,<sup>19</sup> K. S. Park,<sup>43</sup> N. Parslow,<sup>44</sup> L. S. Peak,<sup>44</sup> M. Pernicka,<sup>13</sup> J.-P. Perroud,<sup>20</sup>  
 M. Peters,<sup>9</sup> L. E. Piilonen,<sup>56</sup> A. Poluektov,<sup>2</sup> F. J. Ronga,<sup>10</sup> N. Root,<sup>2</sup> M. Rozanska,<sup>30</sup>  
 H. Sagawa,<sup>10</sup> M. Saigo,<sup>48</sup> S. Saitoh,<sup>10</sup> Y. Sakai,<sup>10</sup> H. Sakamoto,<sup>18</sup> T. R. Sarangi,<sup>10</sup>  
 M. Satapathy,<sup>55</sup> N. Sato,<sup>24</sup> N. Satoyama,<sup>42</sup> O. Schneider,<sup>20</sup> J. Schümann,<sup>29</sup> C. Schwanda,<sup>13</sup>  
 A. J. Schwartz,<sup>6</sup> T. Seki,<sup>51</sup> S. Semenov,<sup>14</sup> K. Senyo,<sup>24</sup> Y. Settai,<sup>5</sup> R. Seuster,<sup>9</sup>  
 M. E. Sevier,<sup>23</sup> T. Shibata,<sup>32</sup> H. Shibuya,<sup>46</sup> B. Shwartz,<sup>2</sup> V. Sidorov,<sup>2</sup> V. Siegle,<sup>38</sup>  
 J. B. Singh,<sup>35</sup> A. Somov,<sup>6</sup> N. Soni,<sup>35</sup> R. Stamen,<sup>10</sup> S. Stanič,<sup>54,†</sup> M. Starič,<sup>15</sup> A. Sugi,<sup>24</sup>  
 A. Sugiyama,<sup>39</sup> K. Sumisawa,<sup>34</sup> T. Sumiyoshi,<sup>51</sup> S. Suzuki,<sup>39</sup> S. Y. Suzuki,<sup>10</sup> O. Tajima,<sup>10</sup>  
 F. Takasaki,<sup>10</sup> K. Tamai,<sup>10</sup> N. Tamura,<sup>32</sup> K. Tanabe,<sup>49</sup> M. Tanaka,<sup>10</sup> G. N. Taylor,<sup>23</sup>  
 Y. Teramoto,<sup>33</sup> X. C. Tian,<sup>36</sup> S. Tokuda,<sup>24</sup> S. N. Tovey,<sup>23</sup> K. Trabelsi,<sup>9</sup> T. Tsuboyama,<sup>10</sup>

T. Tsukamoto,<sup>10</sup> K. Uchida,<sup>9</sup> S. Uehara,<sup>10</sup> T. Uglov,<sup>14</sup> K. Ueno,<sup>29</sup> Y. Unno,<sup>3</sup> S. Uno,<sup>10</sup>  
Y. Ushiroda,<sup>10</sup> G. Varner,<sup>9</sup> K. E. Varvell,<sup>44</sup> S. Villa,<sup>20</sup> C. C. Wang,<sup>29</sup> C. H. Wang,<sup>28</sup>  
J. G. Wang,<sup>56</sup> M.-Z. Wang,<sup>29</sup> M. Watanabe,<sup>32</sup> Y. Watanabe,<sup>50</sup> L. Widhalm,<sup>13</sup>  
Q. L. Xie,<sup>12</sup> B. D. Yabsley,<sup>56</sup> A. Yamaguchi,<sup>48</sup> H. Yamamoto,<sup>48</sup> S. Yamamoto,<sup>51</sup>  
T. Yamanaka,<sup>34</sup> Y. Yamashita,<sup>31</sup> M. Yamauchi,<sup>10</sup> Heyoung Yang,<sup>41</sup> P. Yeh,<sup>29</sup> J. Ying,<sup>36</sup>  
K. Yoshida,<sup>24</sup> Y. Yuan,<sup>12</sup> Y. Yusa,<sup>48</sup> H. Yuta,<sup>1</sup> S. L. Zang,<sup>12</sup> C. C. Zhang,<sup>12</sup> J. Zhang,<sup>10</sup>  
L. M. Zhang,<sup>40</sup> Z. P. Zhang,<sup>40</sup> V. Zhilich,<sup>2</sup> T. Ziegler,<sup>37</sup> D. Žontar,<sup>21,15</sup> and D. Zürcher<sup>20</sup>

(The Belle Collaboration)

<sup>1</sup>*Aomori University, Aomori*

<sup>2</sup>*Budker Institute of Nuclear Physics, Novosibirsk*

<sup>3</sup>*Chiba University, Chiba*

<sup>4</sup>*Chonnam National University, Kwangju*

<sup>5</sup>*Chuo University, Tokyo*

<sup>6</sup>*University of Cincinnati, Cincinnati, Ohio 45221*

<sup>7</sup>*University of Frankfurt, Frankfurt*

<sup>8</sup>*Gyeongsang National University, Chinju*

<sup>9</sup>*University of Hawaii, Honolulu, Hawaii 96822*

<sup>10</sup>*High Energy Accelerator Research Organization (KEK), Tsukuba*

<sup>11</sup>*Hiroshima Institute of Technology, Hiroshima*

<sup>12</sup>*Institute of High Energy Physics,*

*Chinese Academy of Sciences, Beijing*

<sup>13</sup>*Institute of High Energy Physics, Vienna*

<sup>14</sup>*Institute for Theoretical and Experimental Physics, Moscow*

<sup>15</sup>*J. Stefan Institute, Ljubljana*

<sup>16</sup>*Kanagawa University, Yokohama*

<sup>17</sup>*Korea University, Seoul*

<sup>18</sup>*Kyoto University, Kyoto*

<sup>19</sup>*Kyungpook National University, Taegu*

<sup>20</sup>*Swiss Federal Institute of Technology of Lausanne, EPFL, Lausanne*

<sup>21</sup>*University of Ljubljana, Ljubljana*

<sup>22</sup>*University of Maribor, Maribor*

<sup>23</sup>*University of Melbourne, Victoria*

<sup>24</sup>*Nagoya University, Nagoya*

<sup>25</sup>*Nara Women's University, Nara*

<sup>26</sup>*National Central University, Chung-li*

<sup>27</sup>*National Kaohsiung Normal University, Kaohsiung*

<sup>28</sup>*National United University, Miao Li*

<sup>29</sup>*Department of Physics, National Taiwan University, Taipei*

<sup>30</sup>*H. Niewodniczanski Institute of Nuclear Physics, Krakow*

<sup>31</sup>*Nihon Dental College, Niigata*

<sup>32</sup>*Niigata University, Niigata*

<sup>33</sup>*Osaka City University, Osaka*

<sup>34</sup>*Osaka University, Osaka*

<sup>35</sup>*Panjab University, Chandigarh*

<sup>36</sup>*Peking University, Beijing*

<sup>37</sup>*Princeton University, Princeton, New Jersey 08545*

<sup>38</sup>*RIKEN BNL Research Center, Upton, New York 11973*

<sup>39</sup>*Saga University, Saga*

<sup>40</sup>*University of Science and Technology of China, Hefei*

<sup>41</sup>*Seoul National University, Seoul*

<sup>42</sup>*Shinshu University, Matsumoto*

<sup>43</sup>*Sungkyunkwan University, Suwon*

<sup>44</sup>*University of Sydney, Sydney NSW*

<sup>45</sup>*Tata Institute of Fundamental Research, Bombay*

<sup>46</sup>*Toho University, Funabashi*

<sup>47</sup>*Tohoku Gakuin University, Tagajo*

<sup>48</sup>*Tohoku University, Sendai*

<sup>49</sup>*Department of Physics, University of Tokyo, Tokyo*

<sup>50</sup>*Tokyo Institute of Technology, Tokyo*

<sup>51</sup>*Tokyo Metropolitan University, Tokyo*

<sup>52</sup>*Tokyo University of Agriculture and Technology, Tokyo*

<sup>53</sup>*Toyama National College of Maritime Technology, Toyama*

<sup>54</sup>*University of Tsukuba, Tsukuba*

<sup>55</sup>*Utkal University, Bhubaneswer*

<sup>56</sup>*Virginia Polytechnic Institute and State University, Blacksburg, Virginia 24061*

<sup>57</sup>*Yonsei University, Seoul*

## Abstract

We have searched for the leptonic and radiative leptonic  $B$  decays,  $B^+ \rightarrow \mu^+\nu_\mu$ ,  $B^+ \rightarrow e^+\nu_e\gamma$  and  $B^+ \rightarrow \mu^+\nu_\mu\gamma$ . Using a  $140 \text{ fb}^{-1}$  data sample collected with the Belle detector at the KEKB asymmetric  $e^+e^-$  collider, we find no evidence for signals in any mode and set the following preliminary upper limits at 90% confidence level:  $\mathcal{B}(B^+ \rightarrow \mu^+\nu_\mu) < 2.0 \times 10^{-6}$ ,  $\mathcal{B}(B^+ \rightarrow e^+\nu_e\gamma) < 2.2 \times 10^{-5}$  and  $\mathcal{B}(B^+ \rightarrow \mu^+\nu_\mu\gamma) < 2.3 \times 10^{-5}$ .

PACS numbers: 13.25.Hw, 11.30.Er, 12.15.Hh

---

\*on leave from Fermi National Accelerator Laboratory, Batavia, Illinois 60510

†on leave from Nova Gorica Polytechnic, Nova Gorica

## I. INTRODUCTION

In the Standard Model (SM), the fully-leptonic decays  $B^+ \rightarrow \ell^+ \nu_\ell$ , where  $\ell$  represents an electron, muon, or  $\tau$  lepton, are allowed through annihilation into a virtual  $W$  boson. The branching fraction is given by:

$$\mathcal{B}(B^+ \rightarrow \ell^+ \nu_\ell) = \frac{G_F^2 m_B m_\ell^2}{8\pi} \left(1 - \frac{m_\ell^2}{m_B^2}\right)^2 f_B^2 |V_{ub}|^2 \tau_B,$$

where  $G_F$  is the Fermi coupling constant,  $m_B$  and  $m_\ell$  are the masses of the  $B$  meson and lepton,  $\tau_B$  is the  $B$  meson lifetime,  $V_{ub}$  is an element of the Cabibbo-Kobayashi-Maskawa quark mixing matrix [1], and  $f_B$  is the decay constant that parameterizes the overlap of the quark wave functions within the meson. A measurement of this branching fraction, combined with the value of  $|V_{ub}|$  obtained from other decay modes such as  $B \rightarrow \pi \ell \bar{\nu}_\ell$ , allows us to determine  $f_B$ , which is needed to extract  $|V_{td}|$  from measurements of  $B^0 \bar{B}^0$  mixing. The theoretical expectation for the branching fraction of  $B^+ \rightarrow \tau^+ \nu_\tau$  lies in the range  $(1 - 10) \times 10^{-5}$ . Since the branching fraction is proportional to the square of the mass of the charged lepton, the branching fractions for  $B^+ \rightarrow \mu^+ \nu_\mu$  and  $B^+ \rightarrow e^+ \nu_e$  are suppressed by factors of 225 and  $10^7$ , respectively (“*helicity suppression*”). Although branching fractions at these levels are beyond the reach of the Belle experiment with the current data sample, an observation of either of the latter decay modes would be a clear indication of physics beyond the SM. For example, the  $B^+ \rightarrow \ell^+ \nu_\ell$  decay rate may be enhanced in the minimal super-symmetric standard model (MSSM) via intermediate charged Higgs bosons [2] or in the Pati-Salam model of quark-lepton unification [3]. Similarly,  $B^+ \rightarrow \ell^+ \nu_\ell$  may be mediated by scalar super-symmetric particles in R-parity violating extensions of the MSSM [4]. In this paper, we concentrate on the  $\ell = e$  and  $\mu$  modes. The most stringent current upper limits for these modes are  $\mathcal{B}(B^+ \rightarrow e^+ \nu_e) < 1.5 \times 10^{-5}$  [13] and  $\mathcal{B}(B^+ \rightarrow \mu^+ \nu_\mu) < 2.1 \times 10^{-5}$  [14] at the 90% confidence level.

It is natural to extend the  $B^+ \rightarrow \ell^+ \nu_\ell$  searches to the corresponding radiative modes. Because of the additional photon, helicity suppression does not occur in these modes; hence  $B^+ \rightarrow \ell^+ \nu_\ell \gamma$  decays are predicted to occur with rates comparable to or possibly larger than  $B^+ \rightarrow \mu^+ \nu_\mu$  decay. The  $B^+ \rightarrow \ell^+ \nu_\ell \gamma$  decay has been of theoretical interest as a means of probing aspects of the strong and weak interactions of a heavy quark system [5]-[12]. In theory, there are two contributions to  $B^+ \rightarrow \ell^+ \nu_\ell \gamma$ : the internal Bremsstrahlung (IB) process and the structure-dependent (SD) process [5]. In the IB process, a photon is emitted in either the initial or final state. The amplitude for this process is, however, suppressed by both helicity conservation and the electromagnetic coupling to the photon. In the SD process, the photon is produced in the transition of the spin-0  $B^+$  meson to a spin-1 off-shell vector ( $B^{*+}$ ) or axial-vector ( $B'$ ) meson. Helicity suppression is avoided in this spin exchange. In a recent study by Korchemsky, Pirjol, and Yan (KPY) [12], the predicted branching fraction is in the range  $(2 - 5) \times 10^{-6}$ . Current upper limits on these modes are obtained by CLEO:  $\mathcal{B}(B^+ \rightarrow e^+ \nu_e \gamma) < 2.0 \times 10^{-4}$  and  $\mathcal{B}(B^+ \rightarrow \mu^+ \nu_\mu \gamma) < 5.2 \times 10^{-5}$  [15].

In this paper, we present a preliminary search for the leptonic and radiative leptonic  $B$  meson decays  $B^+ \rightarrow \mu^+ \nu_\mu$ ,  $B^+ \rightarrow e^+ \nu_e \gamma$ , and  $B^+ \rightarrow \ell^+ \nu_\ell \gamma$ . A brief description of the Belle detector is given in the next section. The analysis procedure and results are described in Section III for  $B^+ \rightarrow \mu^+ \nu_\mu$  decays and in Section IV for  $B^+ \rightarrow \ell^+ \nu_\ell \gamma$  decays. Throughout this paper, charge conjugation is implied unless stated otherwise.

## II. THE BELLE DETECTOR

The event sample that we analyze for this study corresponds to an integrated luminosity of  $140 \text{ fb}^{-1}$  accumulated at the  $\Upsilon(4S)$  resonance and recorded by the Belle detector at the KEKB  $e^+e^-$  collider [16]. This sample contains 152 million  $B\bar{B}$  pairs. We also use an event sample of  $15 \text{ fb}^{-1}$  integrated luminosity recorded 60 MeV below  $\Upsilon(4S)$  resonance for background determination.

The Belle detector is a large-solid-angle spectrometer based on a 1.5 T superconducting solenoid magnet. Tracking and momentum measurements of charged particles are done with a 3-layer double-sided silicon vertex detector (SVD) and a central drift chamber (CDC). Identification of charged hadrons is provided by a combination of three measurements: specific ionization ( $dE/dx$ ) in the CDC, photon yield in the aerogel threshold Cerenkov counters (ACC), and time-of-flight information from a cylindrical array of 128 scintillation counters (TOF). Photons are detected in an electromagnetic calorimeter (ECL) system made of an array of 8736 CsI(Tl) crystals surrounding the TOF system. Electrons are identified based on the  $dE/dx$  measurement in the CDC, the response of the ACC, and the position, shape and energy of the electromagnetic shower registered in the ECL. Electron identification efficiency is over 95% in the momentum range of this analysis; the fake rate is below 0.5%. Muons are identified by a resistive plate chamber system (KLM) located within the solenoid's external return yoke. Muon identification efficiency is approximately 90% in the momentum range of this analysis; the fake rate is approximately 1%. The Belle detector is described in detail elsewhere[17].

## III. SEARCH FOR $B^+ \rightarrow \mu^+ \nu_\mu$

The main signature for the  $B^+ \rightarrow \mu^+ \nu_\mu$  decay is a single muon having approximately 2.6 GeV/ $c$  momentum. The muon candidate is selected from the charged tracks that are produced near the interaction point (IP), and identified by its penetration depth and profile in KLM. We use only well-identified muons detected in the barrel region of the Belle detector, where muon identification efficiency and fake rate are well understood. Muon candidates that are consistent with being produced via a  $J/\psi \rightarrow \mu^+ \mu^-$  decay are vetoed.

To exploit the large missing energy and momentum of the undetected neutrino in the  $B^+ \rightarrow \mu^+ \nu_\mu$  decay, we require that there should be only one identified lepton in an event, and that the direction of missing momentum be within the detector's fiducial volume ( $|\cos \theta_{\text{miss}}| < 0.88$ , where  $\theta_{\text{miss}}$  is the polar angle of the missing momentum vector relative to the  $z$  axis that is opposite the positron beam line). These requirements make it likely that the signal neutrino is the only undetected particle in the event, so that the missing mass is consistent with zero. We require  $-4.0 < M_{\text{miss}}^2 < 4.3 \text{ (GeV}/c^2)^2$ .

The detected particles in the event other than the signal muon candidate are required to be consistent with a  $B$  decay hypothesis. This is tested using two kinematic variables,  $M_{\text{bc}} \equiv \sqrt{E_{\text{beam}}^2 - (\sum_i \mathbf{p}_i)^2}$  and  $\Delta E \equiv \sum_i E_i - E_{\text{beam}}$  where  $E_{\text{beam}}$  is the beam energy measured in the center-of-mass (CM) frame and the summations are over all detected particles except the signal muon. We require each event to lie within the region  $5.1 \text{ GeV}/c^2 < M_{\text{bc}} < 5.3 \text{ GeV}/c^2$  and  $-2.0 \text{ GeV} < \Delta E < 1.5 \text{ GeV}$ . The formation of this second  $B$  meson's four-momentum permits us to determine the reference frame in which the parent of the signal muon is at rest (" $B$  rest frame"). We reject events for which the muon momentum in the  $B$  rest frame

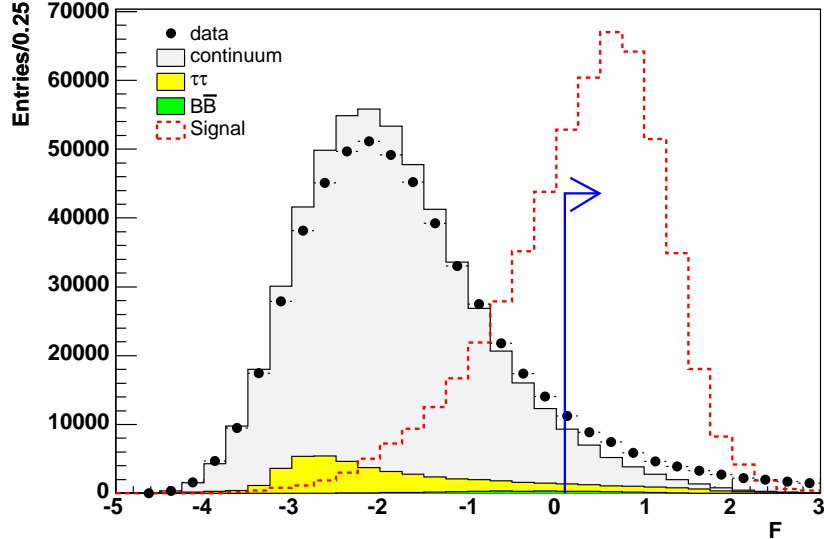


FIG. 1: Distributions of the event shape Fisher discriminant for signal and background MC samples. We require  $\mathcal{F} > 0.1$ .

lies outside the range  $2.58 \text{ GeV}/c < p_\mu^B < 2.8 \text{ GeV}/c$ .

The dominant background arise from  $B \rightarrow X_u \ell \nu_\ell$  decays and from the continuum process  $e^+e^- \rightarrow q\bar{q}$  ( $q = u, d, s, c$ ). There is some additional contamination due to misidentification of a hadron as the signal muon.

The lepton from  $B \rightarrow X_u \ell \nu_\ell$  decays (but not the more abundant  $B \rightarrow X_c \ell \nu_\ell$  decays) can have sufficient energy to populate the  $p_\mu^B$  acceptance window. These events are suppressed by the  $M_{bc}-\Delta E$  cuts, since the second  $\bar{B}$  meson inherits the additional particles associated with the  $X_u$  hadronic system.

Since a  $B$  meson pair produced at the  $\Upsilon(4S)$  resonance has very little kinetic energy in the CM frame ( $\gamma\beta \approx 0.06$ ), the event topology of  $B\bar{B}$  events is spherical while that of the continuum events, where the light quarks are produced with large kinetic energy, tends to be two-jet like. To suppress continuum background, we exploit these event shape differences by combining several Fox-Wolfram event shape moments [18] into a Fisher discriminant [19]  $\mathcal{F}$  whose coefficients are trained using Monte Carlo (MC) simulated event samples to maximize the distinction between signal and background. (See Fig. 1.) We also make use of the angle  $\theta_T$  between the muon momentum and the thrust axis of the second  $B$  meson in the CM frame. We suppress continuum background by requiring  $\mathcal{F} > 0.1$  and  $|\cos \theta_T| < 0.56$ .

Figure 2 shows the  $p_\mu^B$  distributions for signal and background MC events that satisfy all of the above criteria except the  $p_\mu^B$  cut. Signal yield and background contamination are assessed in the two-dimensional subregion  $M_{bc} > 5.26 \text{ GeV}/c^2$  and  $-0.8 \text{ GeV} < \Delta E < 0.4 \text{ GeV}$ . The definition of the signal region, as well as the requirements on  $p_\mu^B$ , event-shape cuts and  $M_{\text{miss}}^2$  are optimized using signal and background MC samples. Using a signal MC sample, the signal detection efficiency is determined to be  $(2.9 \pm 0.1)\%$ .

To estimate the background in the signal region, we define a side-band region by  $5.1 < M_{bc} < 5.24 \text{ GeV}/c^2$  and  $-2.0 < \Delta E < 1.5 \text{ GeV}$ . This and the signal region are indicated in Fig. 3. We fit the  $M_{bc}$  projection of the side-band distribution of the MC background sample to an empirical threshold function (“Argus function”) [20]. Then we estimate the

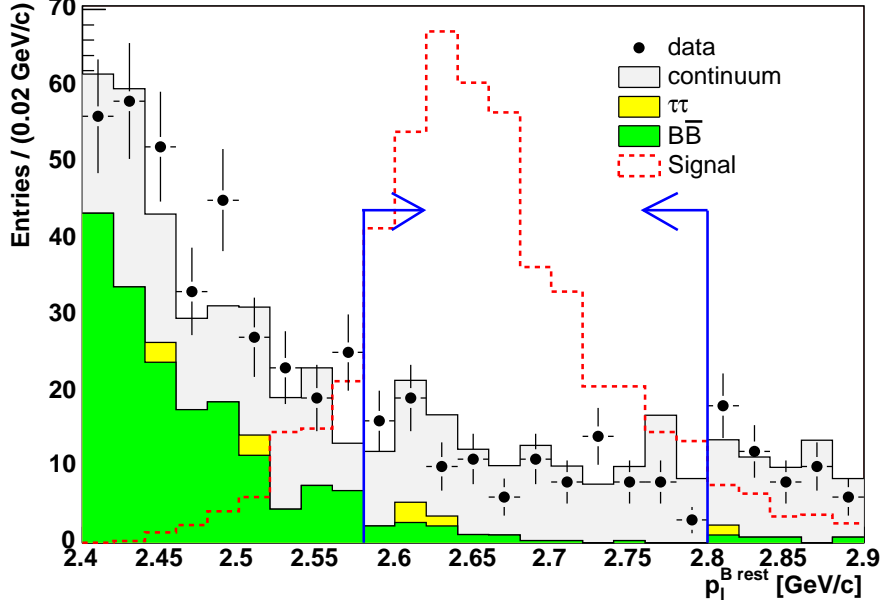


FIG. 2: Distributions of the muon momentum  $p_\mu^B$  in the  $B$  rest frame satisfying all selection criteria except the cut on  $p_\mu^B$ . We require  $2.58 \text{ GeV}/c < p_\mu^B < 2.8 \text{ GeV}/c$ .

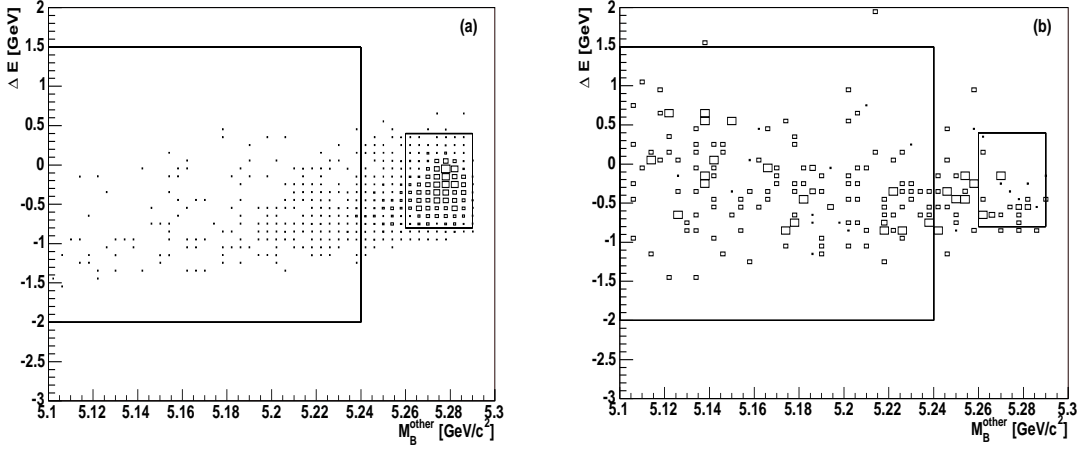


FIG. 3: Distributions in  $M_{bc}-\Delta E$  plane for (a) signal MC events and (b) background MC events satisfying all other event selection cuts. The signal region and side-band region are indicated with rectangles inside the plot.

background in the signal region by fitting the  $M_{bc}$  projection of the data side-band with the same Argus function where the fit parameters except for the overall normalization are fixed to those obtained in the MC fit. The expected background in the signal region, obtained by extrapolating the Argus function, is  $N_{\text{bkg}} = 12.2^{+5.4}_{-5.2}$  events. Assuming no signal events and based on a Poisson fluctuation of background events, we calculate mean expected upper limit as  $1.7 \times 10^{-6}$ , where backgrounds are subtracted.

Figure 4 shows the  $M_{bc}$  distributions for data, background MC, and signal MC events after applying all selection criteria except the  $M_{bc}$  cut. We find 4 events in the  $M_{bc}$  signal region.

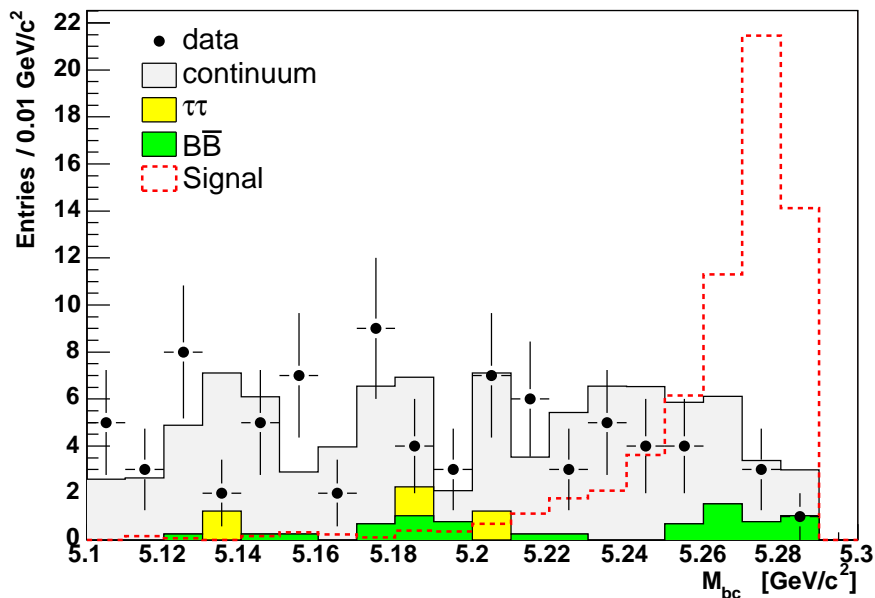


FIG. 4: The  $M_{bc}$  distributions for data (points with error bars) as well as signal and background MC events (histograms) for events satisfying all selection criteria except the cut on  $M_{bc}$ . The signal region is  $M_{bc} > 5.26 \text{ GeV}/c^2$ .

Without subtracting background, we convert this observation and the above expectation for  $N_{\text{bkg}}$  into an upper limit of 7.99 on the signal yield at the 90% confidence level.

The systematic uncertainty in the  $B^+ \rightarrow \ell^+ \nu_\ell$  analysis includes uncertainties in the signal detection efficiency and in the background estimation. Since we do not subtract background in this analysis, we consider only the uncertainty in the efficiency.

The uncertainty in  $N_{B\bar{B}}$  is 0.3%. The uncertainty in track-finding efficiency is 2% per track, and that in muon ID efficiency is 2%. The effect of other event selection cuts is studied by analyzing a calibration sample of fully reconstructed  $B^+ \rightarrow \bar{D}^{(*)0} \pi^+$  decays, where we treat the pion as a signal muon and the  $\bar{D}^{(*)0}$  as the accompanying neutrino. We compare the efficiency of the event selection procedure between data and MC to infer systematic uncertainty in the event selection procedure. The fractional difference of efficiency between data and MC is 5.8%. Including the systematic uncertainty, the signal efficiency is  $(2.9 \pm 0.2)\%$ .

For a conservative upper limit, we reduce the signal efficiency by its error and obtain the following upper limit for the  $B^+ \rightarrow \mu^+ \nu_\mu$  branching fraction at 90% CL:

$$\mathcal{B}(B^+ \rightarrow \mu^+ \nu_\mu) < 2.0 \times 10^{-6}$$



#### IV. SEARCH FOR $B^+ \rightarrow \ell^+ \nu_\ell \gamma$

We search also for the three-body radiative decays  $B^+ \rightarrow e^+ \nu_e \gamma$  and  $B^+ \rightarrow \mu^+ \nu_\mu \gamma$ . The presence of the photon invalidates the monochromaticity constraint on the lepton momentum in the  $B$  rest frame. Nevertheless, theoretical calculations[5] predict the lepton momentum spectrum to peak at the high end of its kinematical range. While the photon's energy is typically much softer than the lepton's, it exceeds that of most photons produced at  $\Upsilon(4S)$  resonance energy

We select the primary muon or electron candidate with CM momentum between 1.8 and 2.8 GeV/ $c$  using the particle identification information described in section II, and the primary photon candidate as the most energetic of the neutral clusters in the ECL (i.e., those not matched to any charged track) above 1.0 GeV that does not appear to be affiliated with a  $\pi^0$  meson. (A photon is considered to be a  $\pi^0$  meson daughter if, when combined with any other photon of energy 100 MeV or more, it gives an invariant mass within  $\pm 15$  MeV/ $c^2$  of the nominal  $\pi^0$  mass.) As before, we require that there be only one identified lepton per event, that the direction of the missing momentum be within the detector's fiducial volume, and that the squared missing mass fall in the range  $-2.0 (\text{GeV}/c^2)^2 < M_{\text{miss}}^2 < 0.8 (\text{GeV}/c^2)^2$ . In addition, we require the charge sum of all detected particles be 0 or  $\pm 1$ .

As before, we calculate  $M_{\text{bc}}$  and  $\Delta E$  for the remaining particles in the event; here, candidates must satisfy  $5.11 \text{ GeV}/c^2 < M_{\text{bc}} < 5.29 \text{ GeV}/c^2$  and  $-0.5 \text{ GeV} < \Delta E < 0.125 \text{ GeV}$ . We also find that the lepton momentum ( $p_\ell$ ) spectrum are different for different sources of backgrounds: the lepton spectrum of  $B\bar{B}$  MC events is peaking near 2.0 GeV/ $c$  and drops out rapidly beyond  $\sim 2.3$  GeV/ $c$  while that of the continuum MC sample is much flatter than the others and reaches to higher momentum regions ( $\sim 3$  GeV/ $c$  or beyond). The signal yield is obtained by fitting the two-dimensional  $p_\ell$ - $M_{\text{bc}}$  distributions.

Continuum background is suppressed by a cut on the normalized second Fox-Wolfram moment (rather than on the Fisher discriminant) of  $R_2 < 0.35$  for  $e^+ \nu_e \gamma$  ( $R_2 < 0.32$  for  $\mu^+ \nu_\mu \gamma$ ). The relative fraction of each background component ( $B\bar{B}$ ,  $X_u \ell \nu_\ell$  and continuum) are determined by fitting the lepton momentum distribution within the  $M_{\text{bc}}$  side-band region of  $5.11 \text{ GeV}/c^2 < M_{\text{bc}} < 5.20 \text{ GeV}/c^2$  to the sum of the three empirically determined shapes for these backgrounds.

For the  $B^+ \rightarrow \mu^+ \nu_\mu \gamma$  mode, Fig. 5 shows the distributions within the signal region of the squared missing mass and photon energy for data and combined background MC (with relative weights equal to those measured in the  $M_{\text{bc}}$  side-band region). In both cases, the shapes of the data and combined background are in good agreement. Similar agreement is seen for the  $B^+ \rightarrow e^+ \nu_e \gamma$  mode.

Before fitting for the signal yield, the procedure is tested on an MC sample made from a mixture of  $B\bar{B}$ , continuum and  $B \rightarrow X_u \ell \nu_\ell$  processes but without including any signal events. The signal yield obtained are consistent with zero for both modes, and we take the corresponding upper limits calculated without systematic uncertainty,  $1.4 \times 10^{-5}$  for  $B^+ \rightarrow e^+ \nu_e \gamma$  mode and  $1.0 \times 10^{-5}$  for  $B^+ \rightarrow \mu^+ \nu_\mu \gamma$ , as the search sensitivity for the corresponding mode.

We perform a binned maximum-likelihood fit to data in the  $p_\ell$ - $M_{\text{bc}}$  plane; the two parameters in this fit are the number of signal and combined-background events. Figure 6 (Fig. 7) shows the projections of the fit onto the  $M_{\text{miss}}^2$  and  $p_\ell$  axes for the  $B^+ \rightarrow e^+ \nu_e \gamma$  ( $B^+ \rightarrow \mu^+ \nu_\mu \gamma$ ) mode. The projection onto  $M_{\text{bc}}$  is made after applying a cut  $2.2 \text{ GeV}/c < p_\ell < 2.8 \text{ GeV}/c$ , and the projection onto  $p_\ell$  is made after applying a cut

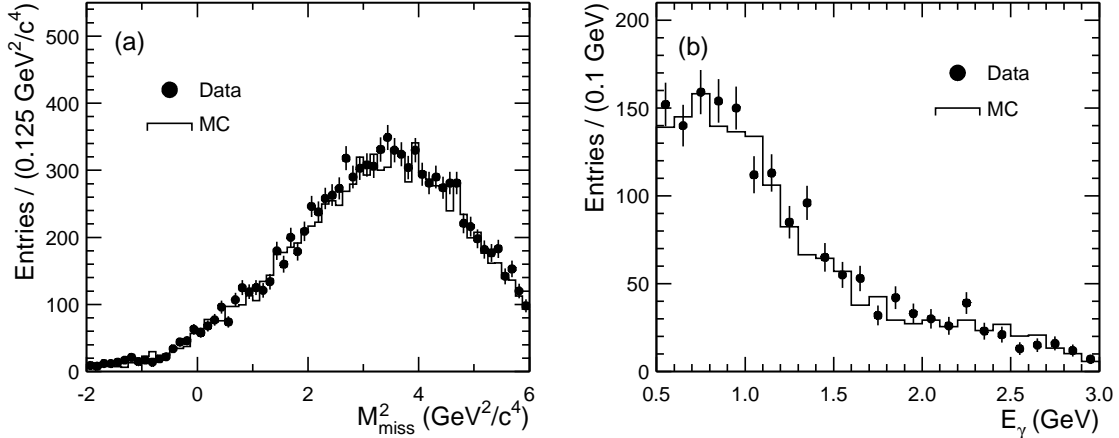


FIG. 5: Data and combined MC distributions of (a) squared missing mass and (b) photon energy for the  $B^+ \rightarrow \mu^+ \nu_\mu \gamma$  mode after application of all event selection criteria except the cut on the displayed quantity.

$$5.26 \text{ GeV}/c^2 < M_{bc} < 5.29 \text{ GeV}/c^2.$$

Since neither mode shows a significant excess above the expected background, we set upper limits by integrating the likelihood as a function of the signal yield. The dotted histograms in Figs. 6 and 7 show the 90% (statistical error only) confidence level (CL) upper limits, added to the background. The fitted yields after efficiency correction are  $970_{-550}^{+610}$  events in the  $B^+ \rightarrow e^+ \nu_e \gamma$  mode, and  $80_{-580}^{+660}$  events in the  $B^+ \rightarrow \mu^+ \nu_\mu \gamma$  mode. Using the statistical error only, the corresponding 90% CL upper limits on the branching fractions are  $1.2 \times 10^{-5}$  for  $B^+ \rightarrow e^+ \nu_e \gamma$ , and  $0.7 \times 10^{-5}$  for  $B^+ \rightarrow \mu^+ \nu_\mu \gamma$ .

Systematic uncertainties related to the signal efficiency are estimated as in the  $B^+ \rightarrow \mu^+ \nu_\mu$  analysis. To be conservative, we reduce the signal efficiency by the systematic error in efficiency.

The systematic uncertainty in the yield extraction has three categories: fitting method, background estimation, and signal modelling. The uncertainty due to the fitting method is estimated by repeating the fit under various scenarios. The systematic effect of background uncertainty is estimated by repeating the fit with each background component fraction changed by one standard deviation. Similarly, the uncertainty due to signal modelling is studied by varying the signal decay parameters in the signal MC generation which is based on the KPY model [12]. In each category, we take the largest deviation from the default procedure as an estimate of systematic uncertainty. Then the three errors are added in quadrature for systematic uncertainty in the yield extraction.

Assuming a Gaussian distribution for the systematic error, we combine the systematic uncertainty in the yield extraction to the statistical error by smearing the original likelihood function obtained in the signal fitting with a Gaussian function based on this error. Then we use this convolved likelihood function to calculate the upper limits. The results, including the reduction of efficiency by the corresponding systematic uncertainty, are:

$$\begin{aligned} \mathcal{B}(B^+ \rightarrow e^+ \nu_e \gamma) &< 2.2 \times 10^{-5} \\ \mathcal{B}(B^+ \rightarrow \mu^+ \nu_\mu \gamma) &< 2.3 \times 10^{-5} . \end{aligned}$$

## V. SUMMARY

In summary, we have searched for  $B^+ \rightarrow \mu^+\nu_\mu$  and  $B^+ \rightarrow \ell^+\nu_\ell\gamma$  decays and found no significant excess in any mode. Therefore, we set preliminary upper limits at the 90% confidence level on the branching fractions of  $\mathcal{B}(B^+ \rightarrow \mu^+\nu_\mu) < 2.0 \times 10^{-6}$ ,  $\mathcal{B}(B^+ \rightarrow e^+\nu_e\gamma) < 2.2 \times 10^{-5}$  and  $\mathcal{B}(B^+ \rightarrow \mu^+\nu_\mu\gamma) < 2.3 \times 10^{-5}$ . The result on  $B^+ \rightarrow \mu^+\nu_\mu$  is more stringent than the existing limit by a factor of three. The  $e^+\nu_e\gamma$  mode upper limit is an improvement from the existing limit by an order of magnitude and the limit on  $\mu^+\nu_\mu\gamma$  is also improved by more than a factor of two.

## Acknowledgments

We thank the KEKB group for the excellent operation of the accelerator, the KEK Cryogenics group for the efficient operation of the solenoid, and the KEK computer group and the National Institute of Informatics for valuable computing and Super-SINET network support. We acknowledge support from the Ministry of Education, Culture, Sports, Science, and Technology of Japan and the Japan Society for the Promotion of Science; the Australian Research Council and the Australian Department of Education, Science and Training; the National Science Foundation of China under contract No. 10175071; the Department of Science and Technology of India; the BK21 program of the Ministry of Education of Korea and the CHEP SRC program of the Korea Science and Engineering Foundation; the Polish State Committee for Scientific Research under contract No. 2P03B 01324; the Ministry of Science and Technology of the Russian Federation; the Ministry of Education, Science and Sport of the Republic of Slovenia; the National Science Council and the Ministry of Education of Taiwan; and the U.S. Department of Energy.

- 
- [1] M. Kobayashi and T. Maskawa, *Prog. Theor. Phys.* **49**, 652 (1973).
  - [2] W.-S. Hou, *Phys. Rev. D* **48**, 2342 (1993).
  - [3] J. C. Pati and A. Salam, *Phys. Rev. D* **8**, 1240 (1973).
  - [4] S. Baek and Y. G. Kim, *Phys. Rev. D* **60**, 077701 (1999).
  - [5] G. Burdman, T. Goldman and D. Wyler, *Phys. Rev. D* **51**, 111 (1995).
  - [6] A. Khodjamirian, G. Stoll, and D. Wyler, *Phys. Lett. B* **358**, 129 (1995).
  - [7] G. Eilam, I. Halperin, and R. R. Mendel, *Phys. Lett. B* **361**, 137 (1995).
  - [8] P. Colangelo, F. De Fazio, and G. Nardulli, *Phys. Lett. B* **372**, 331 (1996).
  - [9] P. Colangelo, F. De Fazio, and G. Nardulli, *Phys. Lett. B* **386**, 328 (1996).
  - [10] D. Atwood, G. Eilam, and A. Soni, *Mod. Phys. Lett. A* **11**, 1061 (1996).
  - [11] C. Q. Geng, C. C. Lih, and Wei-Min Zhang, *Phys. Rev. D* **57**, 5697 (1998).
  - [12] G. P. Korchemsky, D. Pirjol and T.-M. Yan, *Phys. Rev. D* **61**, 114510 (2000).
  - [13] M. Artuso *et al.* (CLEO Collab.), *Phys. Rev. Lett.* **75**, 785 (1995).
  - [14] B. Aubert *et al.* (BaBar Collab.) *Phys. Rev. Lett.* **92**, 221803 (2004).
  - [15] T. Browder *et al.* (CLEO Collab.), *Phys. Rev. D* **56**, 11 (1997).
  - [16] S. Kurokawa and E. Kikutani, *Nucl. Instr. and Meth. A* **499**, 1 (2003), and other papers included in this volume.
  - [17] A. Abashian *et al.* (Belle Collab.), *Nucl. Instr. and Meth. A* **479**, 117 (2002).

- [18] G. C. Fox and S. Wolfram, Phys. Rev. Lett. **41**, 1581 (1978).
- [19] The Fisher discriminant used by Belle, based on modified Fox-Wolfram moments, is described in K. Abe *et al.* (Belle Collab.), Phys. Rev. Lett. **87**, 101801 (2001) and K. Abe *et al.* (Belle Collab.), Phys. Lett. **B 511**, 151 (2001).
- [20] H. Albrecht *et al.* (ARGUS Collab.), Phys. Lett. B **241**, 278 (1990).

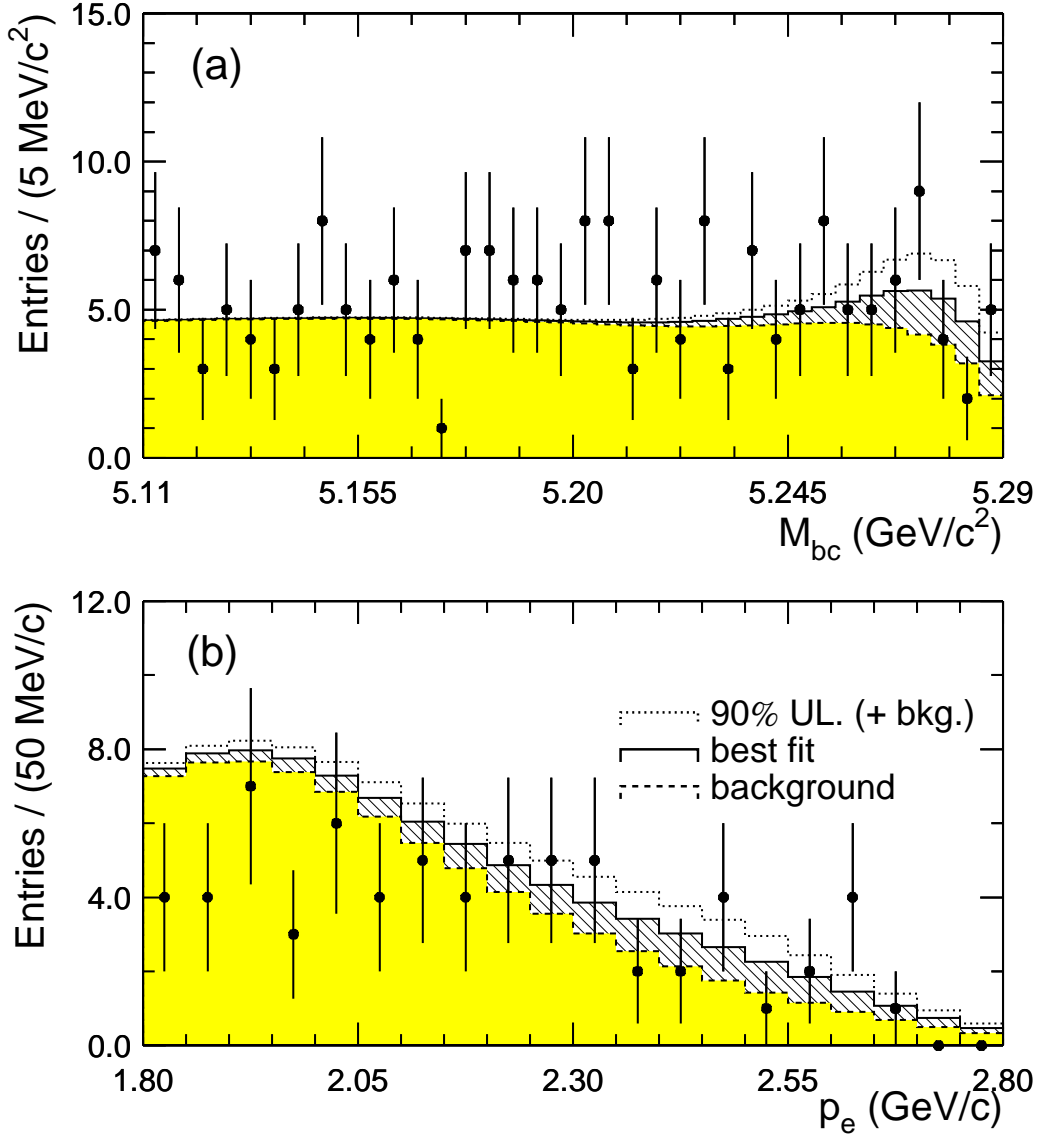


FIG. 6: Distributions of (a) beam constrained  $B$  meson mass and (b) electron momentum for events within the signal region for the  $B^+ \rightarrow e^+ \nu_e \gamma$  mode. The projection onto  $M_{bc}$  is made after applying a cut  $2.2 \text{ GeV}/c < p_e < 2.8 \text{ GeV}/c$ , and the projection onto  $p_e$  is made after applying a cut  $5.26 \text{ GeV}/c^2 < M_{bc} < 5.29 \text{ GeV}/c^2$ . The points represent the data; the curves represent the projections of the fit components. Specifically, the dashed curves show the background only; the solid curves show the background and signal; the dotted curves show an alternate fit with the signal component inflated to its 90% CL upper limit.

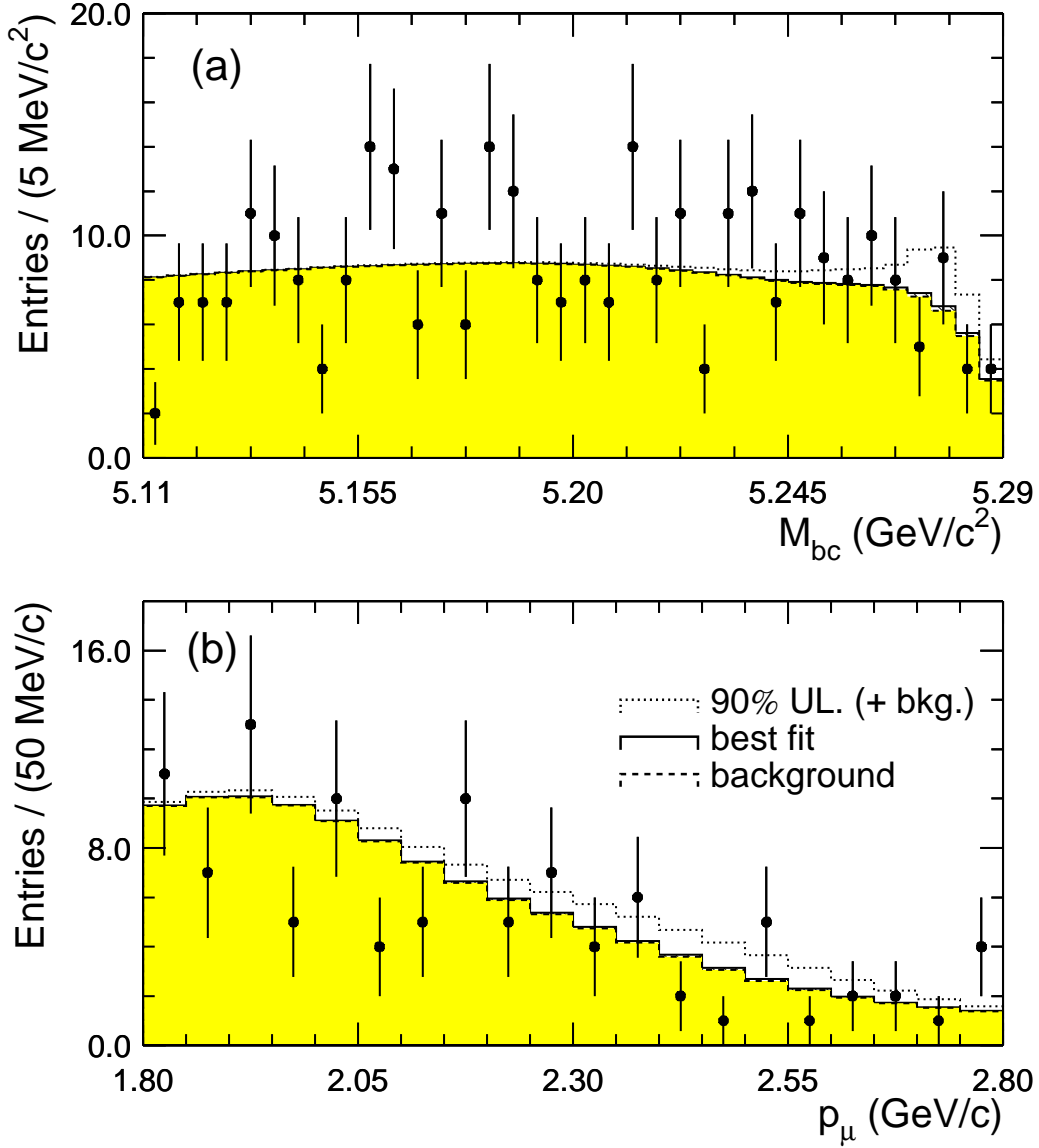


FIG. 7: Distributions of (a) beam constrained  $B$  meson mass and (b) electron momentum for events within the signal region for the  $B^+ \rightarrow \mu^+ \nu_\mu \gamma$  mode. The projection onto  $M_{bc}$  is made after applying a cut  $2.2 \text{ GeV}/c < p_\mu < 2.8 \text{ GeV}/c$ , and the projection onto  $p_\ell$  is made after applying a cut  $5.26 \text{ GeV}/c^2 < M_{bc} < 5.29 \text{ GeV}/c^2$ . The points represent the data; the curves represent the projections of the fit components. Specifically, the dashed curves show the background only; the solid curves show the background and signal; the dotted curves show an alternate fit with the signal component inflated to its 90% CL upper limit.